Author/s:
Tian, Y;Kohn, BP;Qiu, N;Yuan, Y;Hu, S;Gleadow, AJW;Zhang, P

Title:
Eocene to Miocene Out-of-Sequence Deformation in the Eastern Tibetan Plateau: Insights From Shortening Structures in the Sichuan Basin

Date:
2018-02-01

Citation:
Tian, Y., Kohn, B. P., Qiu, N., Yuan, Y., Hu, S., Gleadow, A. J. W. & Zhang, P. (2018). Eocene to Miocene Out-of-Sequence Deformation in the Eastern Tibetan Plateau: Insights From Shortening Structures in the Sichuan Basin. Journal of Geophysical Research Solid Earth, 123 (2), pp.1840-1855. https://doi.org/10.1002/2017JB015049.

Persistent Link:
https://hdl.handle.net/11343/283620

Tian Yuntao (Orcid ID: 0000-0001-5480-9962)
Kohn Barry P. (Orcid ID: 0000-0001-5064-5454)
Gleadow Andrew J.W. (Orcid ID: 0000-0003-0496-0028)

Eocene to Miocene out-of-sequence deformation in the eastern Tibetan Plateau: Insights from shortening structures in the Sichuan Basin

Yuntao Tian [1,2,3], Barry P. Kohn [3], Nansheng Qiu [4], Yusong Yuan [5], Shengbiao Hu [6], Andrew J. W. Gleadow [3], Peizhen Zhang [1,2]

[1] Guangdong Provincial Key Laboratory of Geodynamics and Geohazards, School of Earth Sciences and Engineering, Sun Yat-sen University, Guangzhou 510275, China

[2] *School of Earth Sciences and Engineering, Sun Yat-sen University, Guangzhou 510275, China*

[3] *School of Earth Sciences, The University of Melbourne, Victoria 3010, Australia*

[4] *State Key Laboratory of Petroleum Resource and Prospecting, China University of Petroleum, Beijing 102249, China*

[5] *Petroleum Exploration and Production Research Institute, SINOPEC, Beijing 100083, China*

[6] State Key Laboratory of Lithospheric Evolution, Institute of Geology and Geophysics, Chinese Academy of Sciences, Beijing 100029, China

Key Points:

- Late Eocene-Oligocene phase of shortening in the eastern Sichuan Basin
- Late Miocene tectonic reorganization eastern Tibetan Plateau
- Out-of-sequence deformation triggered probably by enhanced hinterland erosion

This is the author manuscript accepted for publication and has undergone full peer review but has not been through the copyediting, typesetting, pagination and proofreading process, which may lead to differences between this version and the Version of Record. Please cite this article as doi: 10.1002/2017JB015049

Abstract

A distinctive NNE-trending belt of shortening structures dominates the topography and deformation of the eastern Sichuan Basin, ~300 km east of the Tibetan Plateau. Debate continues as to whether the structures resulted from Cenozoic eastward growth of the Tibetan Plateau. A low-temperature thermochronology (AFT and AHe) data set from four deep boreholes and adjacent outcrops intersecting a branch of the shortening structures indicates distinctive differential cooling at ~35-28 Ma across the structure, where stratigraphy has been offset vertically by ~0.8-1.3 km. This result forms the first quantitative evidence for the existence of a late Eocene-Oligocene phase of shortening in the eastern Sichuan Basin, synchronous with the early phase of eastward growth and extrusion of the Tibetan Plateau. Further, a compilation of regional Cenozoic structures reveals a Miocene retreat of deformation from the foreland basin to the hinterland areas. Such a tectonic reorganization indicates that Eocene to Miocene deformation in the eastern Tibetan Plateau is out-of-sequence, and was probably triggered by enhanced erosion in the eastern Tibetan Plateau.

Keywords: Out-of-sequence deformation, Tibetan Plateau; Sichuan Basin; Low-temperature thermochronology; Crustal shortening

1. Introduction

Cenozoic deformation of the Tibetan Plateau, commonly referred to as 'Roof of the World', has been dominated by the north-south India-Eurasia collision since early Cenozoic time [*Yin and Harrison*, 2000; *Tapponnier et al.*, 2001; *Royden et al.*, 2008; *Zhuang et al.*, 2015; *Ding et al.*, 2016]. Numerous lines of evidence suggest that in response to continued convergence the plateau has expanded outwards [*Tapponnier et al.*, 2001; *Clark et al.*, 2005b; *Molnar*, 2005; *Royden et al.*, 2008; *Yuan et al.*, 2013], forming a diverging stress-regime from the collisional belt to plateau margins (Fig. 1a). When and how the expansional strain propagated to the current plateau margins has been hotly debated among several geodynamic models, including: (1) crustal extrusion and shortening model [*Tapponnier et al.*, 2001; *Replumaz and Tapponnier*, 2003; *Hubbard and Shaw*, 2009; *Tian et al*., 2013], (2) lower crustal channel flow [*Bird*, 1991; *Clark et al.*, 2005a; *Royden et al.*, 2008] and (3) distributed shortening model [*Dewey and Bird*, 1970; *England and McKenzie*, 1982; *Dewey et al.*, 1988; *Copley and McKenzie*, 2007]. The first model highlights crustal shortening and lateral extrusion of coherent crustal blocks along major pre-existing mechanically weak belts, and suggests an oblique stepwise rise and growth of the plateau from south to north [*Tapponnier et al.*, 2001; *Replumaz and Tapponnier*, 2003]. The channel flow model emphasizes that following crustal thickening of the central plateau in early Cenozoic time, the lower crust has been redistributed outward by gravitationally-driven ductile flow [*Clark et al.*, 2005a; *Royden et al.*, 2008]. Flow is proposed to have commenced in late Miocene time and spread rapidly to the eastern plateau margin [*Clark et al.*, 2005b]. The

distributed shortening model indicates that the plateau was formed by pure-shear deformation via distributed folding and faulting [*Dewey and Bird*, 1970; *England and McKenzie*, 1982; *Dewey et al.*, 1988; *Copley and McKenzie*, 2007].

The contrasting models have significantly different implications concerning the Cenozoic deformation history of the topographically steep Longmen Shan (the eastern margin of the plateau) and foreland Sichuan Basin to the east (Fig. 1a). The oblique stepwise rise and growth model predicts an Oligocene-Miocene (30-15 Ma) phase of crustal extrusion and shortening in the eastern Tibetan Plateau, which has been accommodated by both the Longmen Shan and the Sichuan basin [*Tapponnier et al.*, 2001; *Replumaz and Tapponnier*, 2003]. The late Cenozoic channel flow model implies that the mechanically strong crust beneath the Sichuan Basin inhibited eastward flow of the lower crust forcing it to extrude upwards along the Longmen Shan [*Clark et al.*, 2005a; *Royden et al.*, 2008]. Therefore, this model predicts minimal or no propagation of late Cenozoic crustal deformation within the Sichuan Basin. The distributed shortening model suggests continuous eastward propagation of shortening driven by topographically produced pressure gradients [*England and McKenzie*, 1982; *Dewey et al.*, 1988; *Copley and McKenzie*, 2007].

In the eastern Sichuan Basin, several parallel belts of NNE-SSE-striking folds and thrusts have developed (Fig. 1b, c). The fold axes and surface trajectories of reverse faults coincide with topographic highs (800-1200 m), ~500 - 800 m higher than the elevations in the surrounding areas (Fig. 1c). Balanced seismic-profiles show ~32 km upper crustal shortening across these

structures [*Li et al*., 2015]. Unfortunately, the timing of development of these structures is poorly constrained. In the eastern Sichuan Basin, the youngest strata involved in these structures is lower Cretaceous (Fig. 1b), requiring deformation to be more recent than early Cretaceous, possibly suggesting Cenozoic shortening. In the southwestern Sichuan Basin, Eocene-Oligocene strata have been found to be involved in the deformation; however, the strata ages are poorly known [*SBGMR*, 1991; *Burchfiel et al.*, 1995]. Therefore, it remains difficult to sustain arguments for extensive Cenozoic shortening over vast areas of the basin.

Given that an explanation for the NNE-SSE-striking structures in the eastern Sichuan Basin has been a key element for testing previous tectonic models, it is crucial to determine the timing and magnitude of shortening of these structures. To address this question the present work applies apatite fission track (AFT) and (U-Th-Sm)/He (AHe) dating, on four deep borehole samples and surface outcrops on different sides of a prominent shortening structure in the eastern Sichuan Basin (Figs. 2, 3).

2. Geological setting

2.1 Adjacent fold-and-thrust belts

The study area is located in the eastern Sichuan Basin. The basin is bounded by four major fold-and-thrust belts, including the southern Qinling, Qiyue Shan, southern Sichuan, and Longmen Shan fold-and-thrust belts to the north, east, south and west, respectively (Fig. 1b). During Mesozoic time, these fold-and-thrust belts accommodated large amount of crustal shortening towards the basin, inverting the basin from a Paleozoic passive continental margin into a

terrestrial foreland basin [*SBGMR*, 1991; *Burchfiel et al.*, 1995]. Such a tectonic inversion resulted from continental collision along the Qinling orogen between the Yangtze and North China blocks, together with associated intra-continental shortening along the Longmen Shan and the Qiyue Shan within the Yangtze block [e.g., *Yan et al.*, 2003; *Dong et al.*, 2011]. Mesozoic crustal shortening along these fold-and-thrust belts continued through to Cretaceous time [*Wang et al.*, 2003; *Yan et al.*, 2003; *Jia et al.*, 2006; *Tian et al.*, 2016].

During the Cenozoic, these deformation belts have been reactivated in different ways. Cenozoic deformation in the Longmen Shan fold-and-thrust belt is characterized by W-E shortening with a minor component of right-lateral faulting, as shown by structural observations [*Burchfiel et al.*, 1995; *Feng et al.*, 2016; *Tian et al.*, 2016], long- and short-term spatial denudation [*Liu-Zeng et al.*, 2011; *Tian et al.*, 2013; *Ansberque et al.*, 2015], and the 2008 Wenchuan Earthquake [*Liu-Zeng et al.*, 2009; *Zhang et al.*, 2010]. The deformation was episodically active during the early Cenozoic [*Tian et al.*, 2016], Eocene-Oligocene and late Miocene [*Wang et al.*, 2012a]. It is worth noting that a thick succession of foreland sediments, expected for the highly-elevated Longmen Shan hinterland, is missing in the range front [*SBGMR*, 1991; *Burchfiel et al.*, 1995]. Only pre-Oligocene and ~600 m thick Pliocene-Quaternary deposits have developed in front of the southern segment of the Longmen Shan [*Burchfiel et al.*, 1995]. This might result from significant denudation in the Sichuan Basin [*Richardson et al.*, 2008; *Tian et al.*, 2012] and the geometry of the Longmen Shan fold-and-thrust belt, characterized by high-angle listric reverse faults [*Tian et al.*, 2013; *Feng et al.*, 2016],

leading to minor tectonic loading over the western margin of the Sichuan Basin [*Feng et al.*, 2016].

Cenozoic deformation in the Qinling was mainly transtensional, as demonstrated by the development of pull-apart basins, such as the NE-striking late Cretaceous-Cenozoic Chengxian Basin in the southern margin of the West Qinling (Fig. 1a) [e.g., *Li et al.*, 2013], grabens, such as the E-striking Cenozoic Weihe Basin in the northern Qinling (Fig. 1a) [e.g., *Liu et al.*, 2013], and half-grabens, such as the late Cretaceous-Cenozoic Hanzhong and Nanyang Basin (Fig. 1a) [e.g., *Wang et al.*, 2003].

Coeval deformation in the internal regions of the Yangtze block, east of the Qiyue Shan fold-and-thrust belt was characterized by N-S extension, as shown by the formation of the Jianghan Basin (Fig. 1a) [e.g., *Liu et al.*, 2003]. The Longmen Shan was reactivated by the eastward growth of the Tibetan Plateau, as shown by enhanced Cenozoic rock exhumation, which has been interpreted as resulting from upper crustal shortening [*Tian et al.*, 2013] or lower crustal channel flow [*Clark et al.*, 2005b; *Enkelmann et al.*, 2006].

2.2. Sichuan Basin

Rocks exposed in the Sichuan Basin show a progressive westward-younging pattern. In the northern, central and eastern parts of the basin, exposed sediments are mainly upper Triassic, lower Jurassic and lower Cretaceous clastic rocks (Figs. 1b and 2). In the southwest and west, surface exposures are mainly upper Cretaceous to Quaternary sediments, with much of the upper Oligocene to lower Pliocene section missing [*SBGMR*, 1991; *Burchfiel et al.*, 1995].

In the eastern Sichuan Basin, Mesozoic strata was strongly deformed, forming several NE-trending parallel folds, characterized by narrow anticlines separated by broad synclines (Fig. 1b) [*Yan et al.*, 2003; *Li et al.*, 2015]. The folds are fault-related, originating from two levels of detachment faults that are located within mechanically weak early Paleozoic and early Triassic deposits (carbonate, shale and gypsum) [*Yan et al.*, 2003; *Jia et al.*, 2006; *Li et al.*, 2015]. These deformation features can be discerned in a seismic profile across the study area (Fig. 3a). The lower detachment and the associated folds and faults involved marine Paleozoic to mid-Triassic strata (Fig. 3a), indicating that deformation occurred in late Triassic time. This deformation marks the initiation of basin tectonic inversion from a passive continental margin into a foreland basin introduced above. The youngest strata involved in the upper detachment and associated structures are Lower Cretaceous (Fig. 3a), suggesting a late Cretaceous – Cenozoic timing. Further, the upper detachment cross-cuts the steeply dipping faults originating from the lower detachment (Fig. 3a), suggesting that the area has accommodated at least two phases of shallow crustal shortening.

Based on the youngest strata involved in the shortening structures, the timing of the latest phase of shortening should be either Cretaceous or Cenozoic or even both. The possibility of Cretaceous deformation is supported by unconformable contacts between Cretaceous and pre-Cretaceous strata developed in areas > 300 km to the east and southeast of the study area outside the Sichuan Basin [*Yan et al.*, 2003]. Evidence for Cenozoic shortening is shown by deformed Tertiary strata in the southwestern Sichuan Basin [*SBGMR*, 1991; *Burchfiel et al.*, 1995].

This study focuses on the Doneyuezhai-Puguang fault, located at the northeast end of one of the NE-striking structures in the eastern Sichuan Basin (Figs. 1c, 2). The surface trajectory of the Dongyuezhai-Puguang fault develops within Lower Jurassic sediments (Fig. 2). Strata on different sides of the structure display opposing dip directions, with steep dip angles adjacent to the structure. Details of the structure have been well-studied by industrial seismic profiles and hydrocarbon exploration, as well as production boreholes [*Ma et al.*, 2007]. As shown on an industrial seismic reflection profile (Fig. 3a), at least two phases of shallow crustal shortening can be recognized: a mid-late Triassic phase involving Paleozoic to Middle Triassic strata and a later phase involving Upper Triassic-Jurassic strata, as outlined above. The Doneyuezhai-Puguang fault comprises a set of faults originating from the upper detachment (Figs. 2 and 3a).

Geothermal studies suggest the basin is colder compared to surrounding areas. Geothermal gradient and heat flow in the Sichuan Basin are 17-33^{o}C/km (average 23^{o}C/km) and 35-69 mW/m^2 (average 53 mW/m^2 average), respectively [*Xu et al.*, 2011], lower than surrounding regions (60-95 mW/m^2) [*Hu et al.*, 2000; *Xu et al.*, 2011]. In the study area in the northeastern Sichuan Basin, the current geothermal gradient is ~18-22 ^{o}C/km [*Xu et al.*, 2011].

3. Previous thermochronological studies

Several thermochronological studies have been carried out in the Sichuan Basin and the surrounding areas to constrain the erosional and deformation history of the region. However, those studies indicate different Cenozoic cooling and erosional histories for the basin, with the

timing of the last phase of enhanced cooling varying from late Miocene to Eocene time. Based on (1) apatite fission-track (AFT) ages of Mesozoic sediments exposed along the Xiongpo anticline in the western Sichuan Basin and (2) thermal history modelling of AFT and apatite (U-Th)/He (AHe) data of individual surface samples from the central Sichuan Basin, *Richardson et al*. [2008] proposed a period of accelerated cooling after ~40 Ma. Thermal history modelling of a group of AHe and AFT data from a borehole from the northern margin of the Sichuan Basin indicated a phase of mid-Cenozoic cooling and erosion commencing at ~30 ± 5 Ma [*Tian et al.*, 2012]. Based on thermal history modelling of AFT data of isolated surface samples, *Li et al*. [2012] suggested that enhanced erosion in the central and southern parts of the basin initiated at ~45 Ma. However, *Shen et al*. [2009] and *Deng et al*. [2013] proposed that the last phase of erosion in the central and eastern Sichuan Basin commenced at 10-20 Ma. Interestingly, applying a similar method to samples close to those reported by *Shen et al*. [2009] in the eastern Sichuan Basin, recent work by *Yang et al*. [2017] suggested a different cooling history with the last phase of erosion commencing at 40-45 Ma.

The variable cooling and erosional histories proposed in those previous studies for a specific part of the basin may result from the observational errors associated with the AFT and AHe data and the non-uniqueness of thermal history modeling for explaining single-sample thermochronological data [*Laslett et al.*, 1987; *Gallagher*, 2012]. One way to maximize the reliability of the reconstructed thermal history is to apply multi-thermochronological methods to a group of samples sharing a similar thermal history, e.g. a set of samples from a vertical

elevation profile or borehole [*Fitzgerald et al.*, 1986; *Gallagher*, 2012], as applied in this work.

4. Sampling, methods and results

4.1. Sampling and methods

Low-temperature thermochronological apatite fission-track and (U-Th-Sm)/He (AFT and AHe) data derived from vertical elevation profiles can provide important constraints on the thermal responses to discrete phases of exhumation [e.g., *Fitzgerald et al.*, 1986]. In this work, to test the possibility of Cenozoic deformation along the Doneyuezhai-Puguang fault, deep samples were collected from four boreholes – two on each side of the shortening structure (Figs. 2 and 3a), between which the distance is as close as <7 km. To maximize the range of elevation and stratigraphic section investigated, surface outcrops adjacent to the boreholes were also sampled.

Each side of the Doneyuezhai-Puguang fault displays similar Mesozoic stratigraphy, indicating similar deposition histories. Further, current borehole strata burial depths are almost identical (Fig. 3b), suggesting they have experienced a similar post-depositional exhumation history. Therefore, the boreholes and surface samples from each side of the structure can be grouped to form two vertical-profiles. One profile from the northwest side of the structure includes the Maoba-1 and -3 boreholes and two outcrop samples (OMB-11, -12). The other profile, located on the southeast side, consists of the Puguang-2 and -5 boreholes and two outcrop samples (OPG-11, -15). For simplicity, these two groups are hereafter named as the MB-profile and PG-profile, respectively. Although the lateral distance between the two groups is as

close as <7 km, the vertical offset between their strata can be as great as 0.8-1.3 km (Figs. 3b), indicating substantial differential uplift and erosion across the Dongyuezhai-Puguang fault.

AFT and AHe analyses were carried out at the University of Melbourne and Commonwealth Scientific and Industrial Research Organization (CSIRO), Australia. Details of experimental methods are presented in the online supporting information.

4.2. Results

All AFT and AHe ages from both profiles are younger than their stratigraphic age (Fig. 4 and Tables 1, S1-S5), with the exception of the AFT age of sample OPG11. This exceptional sample was collected from the youngest strata (lower Cretaceous) in the study area (Fig. 2), and yields an earliest Cretaceous AFT central age (143.3 ± 9.8 Ma) with a relatively higher dispersion (37%) compared to other samples (Table S3). This age overlaps with the depositional age of the host strata, indicating partial thermal resetting of the AFT system. Further, four AHe single-grain ages from this sample range between 67-87 Ma, younger than the stratigraphic age. These observations suggest that the lower Cretaceous strata have been buried to the partial annealing zone of AFT system (~80-100 °C), which is high enough to totally reset the AHe system but not the AFT system [*Farley*, 2002; *Gleadow et al.*, 2002]. Therefore, AFT data from sample OPG11 includes significant age inheritance from the source area and is not discussed further.

On the age versus elevation plot, AFT and AHe data show down-profile decreasing trends for both profiles. The AFT age-elevation plot suggests that at relatively shallow depth levels (< 2 km), ages of the MB-profile are slightly younger than the PG-profile, while overlapping ages are

found at deeper levels (Fig. 4a). Similar age differences are also shown in the AHe age-elevation plot. At near surface depths (<500 m), AHe ages from the MB-profile boreholes are younger (by ~10-20 Ma) and less dispersed than the PG-profile, forming two divergent age-elevation trends (Fig. 4c). Non-projected AFT lengths of the two groups range between 10.07 to 12.47 μm (Fig. 4 and Tables S2, S3). On the plot of age versus effective Uranium content (eU, where eU = U+0.235*Th), no apparent correlation is shown for each sample (Fig. S1).

5. Data interpretation by inverse modeling

5.1 Modeling method

Thermal history modeling of the two thermochronology vertical profiles employed the QTQt program using a Bayesian transdimensional Markov Chain Monte Carlo protocol [*Gallagher*, 2012]. The protocol used the multi-kinetic model of *Ketcham et al.* [2007] for apatite fission-track annealing and radiation damage accumulation and annealing model of *Flowers et al*. [2009] for helium diffusion in apatite. Equivalent radius of each analyzed AHe grain is used in the modelling. For detailed information concerning the sequence of steps and parameter settings used, see *Gallagher* [2012]. For each profile, 0.5 million iterations were run to derive stable inverse model results, as presented in Figure 5.

Reasonable geological constraints can eliminate geologically unreasonable thermal path, and make modeling result more informative [*Ketcham*, 2005; *Gallagher*, 2012]. In this work, the geological constraints used for modeling include: (1) present day temperature for surface

samples (15 ± 10 °C), (2) present day temperature offset between the uppermost and lowermost samples of 45 ± 10 °C and 80 ± 10 °C for the MB- and PG-profiles, respectively, which is calculated by multiplying their depth difference by the present mean geothermal gradient (~20 °C /km) [*Hu et al.*, 2000; *Xu et al.*, 2011]. (3) Given that paleotemperature offset may differ from the present value, a too restrictive prior setup for the offset may artificially bias the thermal modeling results. For this reason, prior paleotemperature offsets for the two profiles are set as 45 ± 15 °C and 80 ± 25 °C, respectively, as calculated using the present geothermal gradient together with a ~40% uncertainty. The large range of geological temperature offset provides sufficient freedom for models to search for the best thermal paths, which most closely match the observations. Considering the possibility of variations in paleogeothermal gradient, the temperature offsets are also allowed to vary over time. (3) A box for mid-late Cretaceous time of 100 ± 20 Ma and a temperature of 80 ± 40 °C was used as a constraint for modeling based on the following two lines of evidence. As suggested by the youngest strata (lower Cretaceous) and previously reported low-temperature thermochronology data [*Richardson et al.*, 2008; *Tian et al.*, 2012], the denudation of the basin commenced in late Cretaceous time. Further, as suggested by the partially reset AFT ages and fully reset AHe ages of sample OPG11, the maximum burial of the youngest strata should be between the total resetting temperatures (~80-120 °C) for the two thermochronological methods.

5.2 Modelling results

Modelling results from the two profiles show distinctly different cooling histories between ~35-28 Ma. Prior to that time, both profiles experienced relatively slow cooling (0.4-0.8 °C/Ma). During that time, the cooling rate of the MB-profile increased by a factor of ten to as high as ~5-8 °C/Ma, which was followed by a period of thermal quiescence (Fig. 5a-1). By contrast, in the PG-profile a steady, slow cooling rate (~0.6-0.8 °C /Ma) persisted over this time range (Fig. 5b-1).

AFT and AHe observations closely match the predictions from the contrasting thermal histories between the two profiles indicated above (Figs. 5a-2 and b-2). For AHe predictions, most are consistent with observations, except for a few grains from some samples. In the MB-profile (Fig. 5a-2), the uppermost sample OMB11 yields a relatively older age (~52 Ma) that evidently does not match the predictions; whereas other four ages (~30-33 Ma) fit well. Moving down the vertical section, sample OMB12 yields nine single grain ages falling between 23-41 Ma; and most match the age predictions (~27-39 Ma), except for two relatively younger grains. Further down the profile, AHe ages of the sample MB1-4 are predicted to range between 25-37 Ma; whereas the observations fall between 20-33 Ma with the youngest age slightly off the predictions. For the lower samples, AHe age predictions are consistent with observations.

In the PG-profile (Fig. 5b-2), the AHe age of the uppermost sample OPG11 is predicted to be between 55-70 Ma, consistent with four of the eight observations (67-75 Ma) at the ±2σ uncertainty level but younger than the three relatively older observations (~85-97 Ma) and older than one evidently younger outlier at ~33 Ma. Deeper down the profile, three observations (38-51 Ma) from sample OPG15 fit the model age predictions (38-53 Ma), leaving the youngest

observation at 26.4 ± 1.3 Ma unexplainable. AHe predictions of other deeper samples are consistent with observations, except for the sample PG5yx, in which the relatively older age at 40.5 ± 1.3 Ma is significantly off the predictions.

The AHe ages that cannot be explained by the thermal history constitute ~15% of the total number of analyses. Such age 'misfits' have been reported in previous studies and may result from several factors, such as U and Th zonation, grain breakage, alpha-implantation or other factors that are difficult to quantify by current routine experimental and modeling methods [*Recanati et al.*, 2017 and references therein]. Below, we focus on discussing implications of the main finding of this work that is the contrasting late Eocene-Oligocene cooling pattern between the two profiles across the Doneyuezhai-Puguang fault.

6. Discussion

6.1. Late Eocene – Oligocene shortening

Differential rates of cooling during ~35-28 Ma between the MB- and PG-profiles suggests that the former experienced ~25-35 $^{\circ}$C more cooling. Assuming a thermal gradient of 20-22 $^{\circ}$C/km, the present value for the study area, the difference in cooling is equivalent to a ~1-1.5 km offset, which is similar to the upward offset and throw of ~0.8-1.3 km of the MB-profile relative to PG-profile across the Doneyuezhai-Puguang fault (Fig. 3). We therefore conclude that the differential cooling and stratigraphic offset results from ESE-verging reverse faulting along the Dongyuezhai-Puguang fault between ~35-28 Ma. This is the first geochronological evidence

reported for dating the Cenozoic phase of shortening in the eastern Sichuan Basin.

The new results are consistent with several geological and thermochronological results in the southeastern Sichuan Basin and the Longmen Shan. First, Eocene strata in the southwestern Sichuan Basin have been involved in folds and reverse faults, indicating post-Eocene shortening [*SBGMR*, 1991; *Burchfiel et al.*, 1995]. Further, low-temperature thermochronology data from Mesozoic strata, involved in the Xiongpo anticline in the southwestern Sichuan Basin, suggests a period of accelerated cooling after ~40 Ma [*Richardson et al.*, 2008], supporting post-late Eocene shortening in the southwestern Sichuan Basin. Moreover, as indicated by thermochronology vertical profile data, exhumation of the central Longmen Shan and Jiulong Shan areas commenced since Eocene time, followed by a phase of accelerated exhumation during the Oligocene [*Wang et al.*, 2012a; *Zhang et al.*, 2016]. These results indicate that late Eocene-Oligocene west-east shortening probably represents a phase of regional deformation that was accommodated by a network of structures extending from the eastern Tibetan Plateau to the eastern Sichuan Basin (Fig. 6).

6.2 Mechanism of foreland shortening

Late Eocene-Oligocene west-east shortening in the eastern Sichuan Basin can be explained by two possible mechanisms. Based on thin-skinned structural models and seismic reflection profiles from the central part of the deformation belt, the structures were first speculated to comprise a series of chevron anticlines originating from an east-dipping detachment [*Yan et al.*,

2003; *Li et al.*, 2015]. In this scenario, the shortening structures in the eastern Sichuan Basin were formed by westward propagation of the Qiyue Shan fold-and-thrust belt (Fig. 7a).

However, surface geological mapping and seismic survey results of the Dongyuezhai-Puguang fault area, located in the northern part of the deformation belt suggest the fault is W-dipping (Figs. 2 and 3). Further, recent seismic reflection studies suggest major tectono-stratigraphic layers are mostly west-dipping across the entire basin [*Gao et al.*, 2016]. These strata are separated by detachments within the mechanically weak early Paleozoic and early Triassic carbonate, shale and gypsum, which have been previously identified from a local seismic survey and surface geological mapping [*Yan et al.*, 2003; *Jia et al.*, 2006]. Therefore, late Eocene-Oligocene west-east shortening in the eastern Sichuan Basin can be alternatively explained by west-dipping reverse faulting originating from a basin-scale detachment (Fig. 7a).

Late Eocene-Oligocene shortening in the eastern Sichuan Basin is consistent with the stepwise growth of the evolution of the Tibetan Plateau [*Tapponnier et al.*, 2001; *Replumaz and Tapponnier*, 2003]. The model suggests that the post-Eocene indentation (~2500-km according to *van Hinsbergen* et al. [2011]) by the Indian sub-continent into Eurasia was partially accommodated by the eastward extrusion and W-E shortening of Sichuan Basin and the South China block during Oligocene-Miocene time [*Tapponnier et al.*, 2001; *Replumaz and Tapponnier*, 2003]. However, the timing of deformation determined by this work slightly predates that of the proposed model, providing a new time constraint for the model. Further, the stepwise growth model proposed that the Sichuan Basin had accommodated ~50 km of W-S shortening

[*Replumaz and Tapponnier*, 2003], which is roughly consistent with recent estimates by *Hubbard and Shaw* [2011] and *Li et al.* [2015]. In the western part of the basin, balanced seismic-sections suggest >20 km shortening [*Hubbard and Shaw*, 2009]. The eastern part of the basin experienced two phases of crustal shortening during the late Triassic and Cretaceous – Cenozoic, with each phase accommodating roughly an equal amount of crustal shortening, measuring ~16 km during each phase [*Li et al.*, 2015]. Considering the possible Cretaceous contribution in forming the upper detachment, it is suggested that the maximum limit of the late Eocene-Oligocene phase of shortening can be estimated as ~16 km. The sum of shortening is close to the estimate by *Replumaz and Tapponnier* [2003].

Deformation in the Qinling to the north and Yangtze block to the east is incompatible with late Eocene-Oligocene shortening in the Sichuan Basin. Cenozoic deformation in the Qinling is mainly transtensional, as indicated by the development of pull-apart basins, half-grabens and grabens in the central and northern marginal areas [*Wang et al.*, 2003; *Li et al.*, 2013; *Liu et al.*, 2013]. (Fig. 1a). Similarly, deformation in the Yangtze block is also characterized by extension during the Cenozoic, as shown by the formation of the Jianghan Basin (~400 km east of the study area, Fig. 1a), which comprises a set of E-W striking half-grabens and grabens [e.g., *Liu et al.*, 2003].

To summarize, Cenozoic transtensional and extensional deformation in the Qingling and Yangtze blocks cannot explain the observed late Eocene-Oligocene shortening in the Sichuan Basin. We conclude that the most likely mechanism for the shallow crustal shortening observed

resulted from the eastward growth of the Tibetan Plateau.

6.3. Late Miocene tectonic reorganization

Compared to regional late Eocene-Oligocene deformation extending from the eastern Tibetan Plateau to the eastern Sichuan Basin, late Miocene deformation is mainly accommodated by the eastern Tibetan Plateau and the western front of the Sichuan Basin (Fig. 6). First, a late Miocene (~10 Ma) phase of rapid exhumation occurred in the central and southern Longmen Shan [*Kirby et al.*, 2002; *Godard et al.*, 2009; *Wang et al.*, 2012a; *Cook et al.*, 2013; *Tian et al.*, 2013], Danba antiform [*Clark et al.*, 2005b; *Jolivet et al.*, 2015], Jiulong Shan [*Zhang et al.*, 2016] Yalong fault [*Wang et al.*, 2012b] and other areas to the south [*Clark et al.*, 2005b; *Ouimet et al.*, 2010], the plateau interior to the west [*Tian et al.*, 2015], and the southwestern Qinling to the northwest [*Enkelmann et al.*, 2006]. This phase of exhumation implies a distinct episode of rock uplift and mountain building in eastern Tibetan Plateau. Further, a large amount of left-lateral strike-slip fault displacement along the Xianshuihe fault, south of the Longmen Shan, also initiated around late Miocene time (~12 Ma) [*Zhang et al.*, 2017] (Fig. 6). Moreover, in contrast to the eastern Sichuan Basin, Cenozoic deformation in the western Sichuan Basin may have continued to late Miocene time, as indicated by a Miocene deposition hiatus and the shortening of Pliocene-Quaternary deposits [*SBGMR*, 1991; *Burchfiel et al.*, 1995; *Li et al.*, 2016]. Therefore, it is likely that during the late Cenozoic, tectonic deformation may have retreated westwards to focus on the eastern Tibetan Plateau and the foreland front (Fig. 6).

As for the eastern Tibetan Plateau, late Miocene tectonic reorganization, shown as reorientation of crustal shortening and concurrent outward growth of high terrains, has also been observed in the northern Tibetan Plateau [e.g., *Yuan et al*., 2013; *Zuza and Yin*, 2016]. *Yuan et al*. [2013] suggested that the reorganization resulted from removal of mantle lithosphere and crustal flow in response to pressure gradients set by evolving differences in elevation. In contrast, *Zuza and Yin* [2016] proposed that tectonic reorganization was triggered by strain redistribution during late Miocene onset or acceleration of strike-slip faulting along major faults.

In the eastern Tibetan Plateau, the late Miocene reorganization of deformation may have resulted from different geodynamic processes. First, the reorganization is consistent with out-of-sequence reverse faulting that develops or remains active in the hinterland of a fold-and-thrust belt (Fig. 7b) [*Morley*, 1988]. One of the mechanisms for out-of-sequence deformation is enhanced erosion in the hinterland [*Morley*, 1988; *Malavieille*, 2010]. This mechanism is applicable to the study area, because the retreat of deformation is accompanied by enhanced erosion in the eastern Tibetan Plateau margin and interior during Miocene time [*Wang et al.*, 2012a; *Tian et al.*, 2013; *Tian et al.*, 2015]. Further, the spatial pattern of late Miocene erosion follows major structures, showing a dependence of rock exhumation along listric reverse faults [*Tian et al.*, 2013; *Tian et al.*, 2015].

Second, the reorganization of deformation is probably inconsistent with the distributed shortening model. This model proposes that the N-S India-Eurasia convergence would produce an eastward topographically driven pressure gradient, which may lead to continuous eastward

shortening [*England and McKenzie*, 1982; *Dewey et al.*, 1988; *Copley and McKenzie*, 2007]. This prediction is apparently incompatible with the late Miocene westward retreat of deformation.

Lastly, *Wang et al*. [2012] presented a model highlighting tectonic transition from early Cenozoic crustal shortening to late Miocene lower crustal channel flow (Fig. 7b). The model argues that lower-crustal material flowing outward from the central plateau is backstopped by the old and strong cratonic lithosphere beneath the Sichuan Basin, pushing up on the crust above and maintaining high topography through sustained dynamic support along the Longmen Shan. Therefore, this model predicts sub-vertical movements originating from the deeper crust beneath the Longmen Shan, and precludes significant horizontal crustal shortening underneath the Longmen Shan and Sichuan Basin [*Clark et al.*, 2005a; *Royden et al.*, 2008]. The model appears to explain the late Miocene tectonic reorganization and geophysical observations, such as negative seismic velocity anomalies in the middle-lower crust [*Clark et al.*, 2005a; *Royden et al.*, 2008], but inconsistent with some other geological observations reported recently. First, the long-term average erosion pattern constructed from thermochronology data is consistent with a structural configuration characterized by a set of listric reverse faults, which differs from the frontal thrusting and hinterland extension architecture required by the channel flow model [*Tian et al.*, 2013]. Further, co- and post-seismic deformation resulting from the 2008 Wenchuan Earthquake is also consistent with a listric reverse fault model [*Liu-Zeng et al.*, 2009; *Xu et al.*, 2009; *Zhang et al.*, 2010]. Finally, seismic reflection profiles across the Longmen Shan suggest structure styles consistent with crustal shortening [*Hubbard and Shaw*, 2011; *Guo et al.*, 2013;

Feng et al., 2016].

7. Conclusions

A low-temperature thermochronology (AFT and AHe) data set from four deep boreholes and four adjacent outcrop samples intersecting a prominent shortening structure in the eastern Sichuan Basin, some ~300 km east of the Tibetan Plateau, offers important insights into the timing of formation of a belt of NNE-trending folds and thrusts in shallow crust. Contrasting thermal histories across the structure identify a distinctive cooling episode between ~35-28 Ma, which for the first time, constrains the timing of the Cenozoic shortening along this structural belt. This timing is consistent with that reported from the southwestern Sichuan Basin and in the Longmen Shan. Therefore, it is concluded that a regional phase of west-east shortening in the eastern Tibetan Plateau occurred in late Eocene-Oligocene time. A compilation of Cenozoic structures in the region indicates a late Miocene retreat of deformation westwards to the eastern Tibetan Plateau, suggesting out-of-sequence deformation in this area between the Eocene and Miocene. This deformation pattern could be triggered by a phase of rapid Miocene erosion in the Longmen Shan and hinterland as indicated by thermochronological data reported previously.

Acknowledgements

Funding for this research was provided by Chinese 1000 Young Talents Program, National Natural Science Foundation of China (NSFC) grant no. 41772211 and the Guangdong Province

Introduced Innovative R&D Team of “Geological Processes and Natural Disasters around the South China Sea” (2016ZT06N331). The University of Melbourne thermochronology laboratory receives infrastructure support from the Australian Research Council and the AuScope Program of NCRIS. The authors are grateful to Chuanqing Zhu, Ming Xu, Jianzhong Qin and Tenger for their field assistance, and to Abaz Alimanovic, Brent McInnes and Noreen Evans for technical assistance with (U-Th-Sm)/He dating. Constructive reviews by Bastian Wauschkuhn and Andrew Zuza clarified many points in this article. A more detailed discussion of the analytical methodology can be found in the supporting information [*Farley et al.*, 1996; *House et al.*, 2000; *Galbraith*, 2005; *Ketcham et al.*, 2007; *Gleadow et al*., 2009; *Jochum et al*., 2011]. The data for this paper are included in the manuscript and the associated supporting information.

REFERENCES CITED

Ansberque, C., V. Godard, O. Bellier, J. De Sigoyer, J. Liu-Zeng, X. Xu, Z. Ren, Y. Li, and A. S. T. E. R. Team (2015), Denudation pattern across the Longriba fault system and implications for the geomorphological evolution of the eastern Tibetan margin, *Geomorphology*, *246*, 542-557.

Bird, P. (1991), Lateral Extrusion of Lower Crust From Under High Topography in the Isostatic Limit, J. Geophys. Res., 96(B6), 10275-10286.

Burchfiel, B. C., Z. Chen, Y. Liu, and L. H. Royden (1995), Tectonics of the Longmen Shan and adjacent regions, central China, *Int. Geol. Rev.*, *37*(8), 661-735.

Clark, M. K., J. W. M. Bush, and L. H. Royden (2005a), Dynamic topography produced by lower crustal flow against rheological strength heterogeneities bordering the Tibetan Plateau, *Geophy. J. Int.*, *162*(2), 575-590.

Clark, M. K., M. A. House, L. H. Royden, K. X. Whipple, B. C. Burchfiel, X. Zhang, and W. Tang (2005b), Late Cenozoic uplift of southeastern Tibet, *Geology*, *33*(6), 525-528.

Cook, K. L., L. H. Royden, B. C. Burchfiel, Y.-H. Lee, and X. Tan (2013), Constraints on Cenozoic tectonics in the southwestern Longmen Shan from low-temperature thermochronology, *Lithosphere*, *5*(4), 393-406.

Copley, A., and D. McKenzie (2007), Models of crustal flow in the India-Asia collision zone, Geophy. J. Int., 169(2), 683-698.

Deng, B., S.-g. Liu, Z.-w. Li, L. F. Jansa, S. Liu, G.-z. Wang, and W. Sun (2013), Differential exhumation at eastern margin of the Tibetan Plateau, from apatite fission-track thermochronology, *Tectonophysics*, *591*, 98-115.

Dewey, J. F., and J. M. Bird (1970), Mountain belts and the new global tectonics, J. Geophys. Res., 75(14), 2625-2647.

Dewey, J. F., R. M. Shackleton, C. Chengfa, and S. Yiyin (1988), The tectonic evolution of the Tibetan Plateau, Philosophical Transactions of the Royal Society of London. Series A, Mathematical and Physical Sciences, 327(1594), 379.

Ding, L., M. Qasim, I. A. K. Jadoon, M. A. Khan, Q. Xu, F. Cai, H. Wang, U. Baral, and Y. Yue (2016), The India–Asia collision in north Pakistan: Insight from the U–Pb detrital zircon provenance of Cenozoic foreland basin, *Earth Planet. Sci. Lett.*, *455*, 49-61.

Dong, Y., G. Zhang, F. Neubauer, X. Liu, J. Genser, and C. Hauzenberger (2011), Tectonic evolution of the Qinling orogen, China: Review and synthesis, *J. Asian Earth Sci.*, *41*(3), 213-237.

England, P., and D. McKenzie (1982), A thin viscous sheet model for continental deformation, Geophysical Journal of the Royal Astronomical Society, 70(2), 295-321.

Enkelmann, E., L. Ratschbacher, R. Jonckheere, R. Nestler, M. Fleischer, R. Gloaguen, B. R. Hacker, Y. Q. Zhang, and Y. S. Ma (2006), Cenozoic exhumation and deformation of northeastern Tibet and the Qinling: Is Tibetan lower crustal flow diverging around the Sichuan Basin?, *Geol. Soc. Am. Bull.*, *118*(5-6), 651-671.

Farley, K. A. (2002), (U-Th)/He Dating: Techniques, Calibrations, and Applications, *Rev. Mineral. Geochem.*, *47*(1), 819-844.

Farley, K. A., R. A. Wolf, and L. T. Silver (1996), The effects of long alpha-stopping distances on (U-Th)/He ages, *Geochim. Cosmochim. Acta*, *60*(21), 4223-4229.

Feng, S.-y., P.-z. Zhang, B.-j. Liu, M. Wang, S.-b. Zhu, Y.-k. Ran, W.-t. Wang, Z.-q. Zhang, W.-j. Zheng, D.-w. Zheng, H.-p. Zhang, and X.-f. Tian (2016), Deep crustal deformation of the

Longmen Shan, eastern margin of the Tibetan Plateau, from seismic reflection and Finite Element modeling, *JGR, 121*(2), 767-787.

Fitzgerald, P. G., M. Sandiford, P. J. Barrett, and A. J. W. Gleadow (1986), Asymmetric extension associated with uplift and subsidence in the Transantarctic Mountains and Ross Embayment, *Earth Planet. Sci. Lett., 81*(1), 67-78.

Flowers, R. M., R. A. Ketcham, D. L. Shuster, and K. A. Farley (2009), Apatite (U-Th)/He thermochronometry using a radiation damage accumulation and annealing model, *Geochim. Cosmochim. Acta, 73*(8), 2347-2365.

Galbraith, R. F. (2005), *Statistics for fission track analysis*, 240 pp., Chapman & Hall/CRC, Boca Raton, Florida.

Gallagher, K. (2012), Transdimensional inverse thermal history modelling for quantitative thermochronology, *J. Geophys. Res., 117, B02408, doi:10.1029/2011JB008825.*

Gao, R., C. Chen, H. Wang, Z. Lu, L. Brown, S. Dong, S. Feng, Q. Li, W. Li, Z. Wen, and F. Li (2016), SINOPROBE deep reflection profile reveals a Neo-Proterozoic subduction zone beneath Sichuan Basin, *Earth Planet. Sci. Lett., 454*, 86-91.

Gleadow, A. J. W., D. X. Belton, B. P. Kohn, and R. W. Brown (2002), Fission track dating of phosphate minerals and the thermochronology of apatite, *Rev. Mineral. Geochem., 48*, 579-630.

Gleadow, A. J. W., S. J. Gleadow, D. X. Belton, B. P. Kohn, M. S. Krochmal, and R. W. Brown (2009), Coincidence mapping - a key strategy for the automatic counting of fission tracks in natural minerals, Geological Society, London, Special Publications, 324(1), 25-36.

Godard, V., R. Pik, J. Lavé, R. Cattin, B. Tibari, J. de Sigoyer, M. Pubellier, and J. Zhu (2009), Late Cenozoic evolution of the central Longmen Shan, eastern Tibet: Insight from (U-Th)/He thermochronometry, *Tectonics, 28, doi:10.1029/2008TC002407*.

Guo, X., R. Gao, G. Randy Keller, X. Xu, H. Wang, and W. Li (2013), Imaging the crustal structure beneath the eastern Tibetan Plateau and implications for the uplift of the Longmen Shan range, *Earth Planet. Sci. Lett., 379*(0), 72-80.

Hintersberger, E., R. C. Thiede, and M. R. Strecker (2011), The role of extension during brittle deformation within the NW Indian Himalaya, Tectonics, 30(3), TC3012.

House, M. A., K. A. Farley, and D. Stockli (2000), Helium chronometry of apatite and titanite using Nd-YAG laser heating, *Earth Planet. Sci. Lett., 183*(3-4), 365-368.

Hu, S. B., L. J. He, and J. Y. Wang (2000), Heat flow in the continental area of China: a new data set, *Earth Planet. Sci. Lett.*, *179*(2), 407-419.

Hubbard, J., and J. H. Shaw (2009), Uplift of the Longmen Shan and Tibetan plateau, and the 2008 Wenchuan (M = 7.9) earthquake, Nature, 458(7235), 194-197.

Jia, D., G. Q. Wei, Z. X. Chen, B. L. Li, Q. Zen, and G. Yang (2006), Longmen Shan fold-thrust belt and its relation to the western Sichuan Basin in central China: New insights fiom hydrocarbon exploration, *AAPG Bull.*, *90*(9), 1425-1447.

Jochum, K. P., U. Weis, B. Stoll, D. Kuzmin, Q. Yang, I. Raczek, D. E. Jacob, A. Stracke, K. Birbaum, D. A. Frick, D. Günther, and J. Enzweiler (2011), Determination of Reference Values for NIST SRM 610–617 Glasses Following ISO Guidelines, Geostand. Geoanal. Res., 35(4), 397-429.

Jolivet, M., F. Roger, Z. Q. Xu, J. L. Paquette, and H. Cao (2015), Mesozoic–Cenozoic evolution of the Danba dome (Songpan Garzê, East Tibet) as inferred from LA-ICPMS U–Pb and fission-track data, *J. Asian Earth Sci.*, *102*, 180-204.

Ketcham, R. A. (2005), Forward and Inverse Modeling of Low-Temperature Thermochronometry Data, *Rev. Mineral. Geochem.*, *58*(1), 275-314.

Ketcham, R. A., A. Carter, R. A. Donelick, J. Barbarand, and A. J. Hurford (2007), Improved modeling of fission-track annealing in apatite, *Am. Mineral.*, *92*(5-6), 799-810.

Kirby, E., P. W. Reiners, M. A. Krol, K. X. Whipple, K. V. Hodges, K. A. Farley, W. Q. Tang, and Z. L. Chen (2002), Late Cenozoic evolution of the eastern margin of the Tibetan Plateau: Inferences from Ar-40/Ar-39 and (U-Th)/He thermochronology, *Tectonics, doi:10.1029/2000TC001246*.

Laslett, G., P. F. Green, I. Duddy, and A. Gleadow (1987), Thermal annealing of fission tracks in apatite 2. A quantitative analysis, *Chem. Geol.*, *65*(1), 1-13.

Li, C., D. He, Y. Sun, J. He, and Z. Jiang (2015), Structural characteristic and origin of intra-continental fold belt in the eastern Sichuan basin, South China Block, *J. Asian Earth Sci.*, *111*, 206-221.

Li, W., Y. Dong, A. Guo, X. Liu, Y. Liu, X. Zha, and K. Zhang (2013), Sedimentary fill history of the Huicheng Basin in the West Qinling Mountains and associated constraints on Mesozoic intracontinental tectonic evolution, *Sci. China Earth Sci.*, *56*(10), 1639-1653.

Li, Z., J. Liu‐Zeng, D. Jia, C. Sun, W. Wang, Z. Yuan, and B. Liu (2016), Quaternary activity of

the range front thrust system in the Longmen Shan piedmont, China, revealed by seismic imaging and growth strata, *Tectonics*, *35*.

Li, Z.-W., S. Liu, H. Chen, B. Deng, M. Hou, W. Wu, and J. Cao (2012), Spatial variation in Meso-Cenozoic exhumation history of the Longmen Shan thrust belt (eastern Tibetan Plateau) and the adjacent western Sichuan basin: Constraints from fission track thermochronology, *J. Asian Earth Sci.*, *47*(0), 185-203.

Liu, J., P. Zhang, R. O. Lease, D. Zheng, J. Wan, W. Wang, and H. Zhang (2013), Eocene onset and late Miocene acceleration of Cenozoic intracontinental extension in the North Qinling range–Weihe graben: Insights from apatite fission track thermochronology, *Tectonophysics*, *584*(0), 281-296.

Liu, S., P. L. Heller, and G. Zhang (2003), Mesozoic basin development and tectonic evolution of the Dabieshan orogenic belt, central China, *Tectonics*, *22*(4), n/a-n/a.

Liu-Zeng, J., L. Wen, M. Oskin, and L. Zeng (2011), Focused modern denudation of the Longmen Shan margin, eastern Tibetan Plateau, *Geochemistry Geophysics Geosystems*, *12*(11), 7380-7399.

Liu-Zeng, J., Z. Zhang, L. Wen, P. Tapponnier, J. Sun, X. Xing, G. Hu, Q. Xu, L. Zeng, L. Ding, C. Ji, K. W. Hudnut, and J. van der Woerd (2009), Co-seismic ruptures of the 12 May 2008, Ms 8.0 Wenchuan earthquake, Sichuan: East-west crustal shortening on oblique, parallel thrusts along the eastern edge of Tibet, *Earth Planet. Sci. Lett.*, *286*(3-4), 355-370.

Ma, Y., X. Guo, T. Guo, R. Huang, X. Cai, and G. Li (2007), The Puguang gas field: New giant discovery in the mature Sichuan Basin, southwest China, *AAPG Bull.*, *91*(5), 627-643.

Malavieille, J. (2010), Impact of eosion, sedimentation, and structural heritage on the structure and kinematics of orogenic wedges: Analog models and case studies, *Gsa Today*, *20*(1), 4-10.

Molnar, P. (2005), Mio-Pliocene growth of the Tibetan Plateau and evolution of East Asian climate, *Palaeontologia Electronica*, *8*(1), 1-23.

Morley, C. K. (1988), Out-of-Sequence Thrusts, *Tectonics*, *7*(3), 539–561.

Ouimet, W., K. Whipple, L. Royden, P. Reiners, K. Hodges, and M. Pringle (2010), Regional incision of the eastern margin of the Tibetan Plateau, *Lithosphere*, *2*(1), 50-63.

Recanati, A., C. Gautheron, J. Barbarand, Y. Missenard, R. Pinna-Jamme, L. Tassan-Got, A. Carter, E. Douville, L. Bordier, M. Pagel, and K. Gallagher (2017), Helium trapping in apatite damage: Insights from (U-Th-Sm)/He dating of different granitoid lithologies, *Chem. Geol.*,

470(Supplement C), 116-131.

Replumaz, A., and P. Tapponnier (2003), Reconstruction of the deformed collision zone Between India and Asia by backward motion of lithospheric blocks, *J. Geophys. Res., 108(B6), 2285, doi:10.1029/2001JB000661*.

Richardson, N. J., A. L. Densmore, D. Seward, A. Fowler, M. Wipf, M. A. Ellis, L. Yong, and Y. Zhang (2008), Extraordinary denudation in the Sichuan Basin: Insights from low-temperature thermochronology adjacent to the eastern margin of the Tibetan Plateau, *J. Geophy. Res.,113, B04409, doi:10.1029/2006JB004739.*

Royden, L. H., B. C. Burchfiel, and R. D. van der Hilst (2008), The Geological Evolution of the Tibetan Plateau, *Science*, *321*(5892), 1054-1058.

SBGMR (Sichuan Bureau of Geology and Mineral Resources) (1991), *Regional Geology of Sichuan Province*, 728 pp., Geol. Publ. House, Beijing.

Shen, C., L. Mei, and S. Xu (2009), Fission track dating of mesozoic sandstones and its tectonic significance in the Eastern Sichuan Basin, China, *Radiat. Meas.*, *44*(9-10), 945-949.

Tang, D. Q., L. J. Wang, T. Zeng, and X. L. Feng (2008), Tectonic Evolvement Function to Oil and Gas Pool's Reformation in Xuanhan-Daxian Area, Northeastern Sichuan Basin, *Geoscience*, *22*, 230-238.

Tapponnier, P., Z. Xu, F. Roger, B. Meyer, N. Arnaud, G. Wittlinger, and J. Yang (2001), Oblique Stepwise Rise and Growth of the Tibet Plateau, *Science*, *294*(5547), 1671-1677.

Tian, Y., B. P. Kohn, A. J. W. Gleadow, and S. Hu (2013), Constructing the Longmen Shan eastern Tibetan Plateau margin: Insights from low-temperature thermochronology, *Tectonics*, *32*(3), 576-592.

Tian, Y., B. P. Kohn, S. Hu, and A. J. W. Gleadow (2015), Synchronous fluvial response to surface uplift in the eastern Tibetan Plateau: Implications for crustal dynamics, *Geophys. Res. Lett.*, *42*(1), 29-35.

Tian, Y., B. P. Kohn, C. Zhu, M. Xu, S. Hu, and A. J. W. Gleadow (2012), Post-orogenic evolution of the Mesozoic Micang Shan Foreland Basin system, central China, *Basin Res.*, *24*(1), 70-90.

Tian, Y., B. P. Kohn, D. Phillips, S. Hu, A. J. W. Gleadow, and A. Carter (2016), Late Cretaceous–earliest Paleogene deformation in the Longmen Shan fold-and-thrust belt, eastern Tibetan Plateau margin: Pre-Cenozoic thickened crust?, *Tectonics*, *35*(10), 2293-2312.

Wang, E., Q. Meng, B. C. Burchfiel, and G. Zhang (2003), Mesozoic large-scale lateral extrusion, rotation, and uplift of the Tongbai-Dabie Shan belt in east China, *Geology*, *31*(4), 307-310.

Wang, E., E. Kirby, K. P. Furlong, M. van Soest, G. Xu, X. Shi, P. J. J. Kamp, and K. V. Hodges (2012a), Two-phase growth of high topography in eastern Tibet during the Cenozoic, *Nat. Geosci.*, *5*(9), 640-645.

Wang, S., G. Jiang, T. Xu, Y. Tian, D. Zheng, and X. Fang (2012b), The Jinhe–Qinghe fault—An inactive branch of the Xianshuihe–Xiaojiang fault zone, Eastern Tibet, *Tectonophysics*, *544-545*, 93-102.

Xu, M., C. Zhu, Y. Tian, S. Rao, and S. Hu (2011), Borehole temperature logging and characteristics of subsurface temperature in Sichuan Basin, *Chin. J. Geophys.*, *54*(4), 1052-1060.

Xu, X., X. Wen, G. Yu, G. Chen, Y. Klinger, J. Hubbard, and J. Shaw (2009), Coseismic reverse- and oblique-slip surface faulting generated by the 2008 Mw 7.9 Wenchuan earthquake, China, *Geology*, *37*(6), 515-518.

Yan, D., M. Zhou, H. Song, X. Wang, and J. Malpas (2003), Origin and tectonic significance of a Mesozoic multi-layer over-thrust system within the Yangtze Block (South China), *Tectonophysics*, *361*(3-4), 239-254.

Yang, Z., C. Shen, L. Ratschbacher, E. Enkelmann, R. Jonckheere, B. Wauschkuhn, and Y. Dong (2017), Sichuan Basin and beyond: Eastward foreland growth of the Tibetan Plateau from an integration of Late Cretaceous-Cenozoic fission track and (U-Th)/He ages of the eastern Tibetan Plateau, Qinling, and Daba Shan, *JGR*, *122*(6), 4712-4740.

Yin, A., and T. M. Harrison (2000), Geologic Evolution of the Himalayan-Tibetan Orogen, *Annu. Rev. Earth Planet. Sci.*, *28*(1), 211-280.

Yuan, D.-Y., W.-P. Ge, Z.-W. Chen, C.-Y. Li, Z.-C. Wang, H.-P. Zhang, P.-Z. Zhang, D.-W. Zheng, W.-J. Zheng, W. H. Craddock, K. E. Dayem, A. R. Duvall, B. G. Hough, R. O. Lease, J.-D. Champagnac, D. W. Burbank, M. K. Clark, K. A. Farley, C. N. Garzione, E. Kirby, P. Molnar, and G. H. Roe (2013), The growth of northeastern Tibet and its relevance to large-scale continental geodynamics: A review of recent studies, *Tectonics*, 2013TC003348.

Zhang, H., M. E. Oskin, J. Liu-Zeng, P. Zhang, P. W. Reiners, and P. Xiao (2016), Pulsed exhumation of interior eastern Tibet: Implications for relief generation mechanisms and the origin of high-elevation planation surfaces, *Earth Planet. Sci. Lett.*, *449*, 176-185.

Zhang, P., Z. Shen, M. Wang, W. Gan, R. Burgmann, P. Molnar, Q. Wang, Z. Niu, J. Sun, J. Wu, S. Hanrong, and Y. Xinzhao (2004), Continuous deformation of the Tibetan Plateau from global

positioning system data, Geology, 32(9), 809-812.

Zhang, P.-Z., X.-z. Wen, Z.-K. Shen, and J.-h. Chen (2010), Oblique, High-Angle, Listric-Reverse Faulting and Associated Development of Strain: The Wenchuan Earthquake of May 12, 2008, Sichuan, China, *Annu. Rev. Earth Planet. Sci.*, *38*(1), 353-382.

Zhang, Y.-Z., A. Replumaz, P. H. Leloup, G.-C. Wang, M. Bernet, P. van der Beek, J. L. Paquette, and M.-L. Chevalier (2017), Cooling history of the Gongga batholith: Implications for the Xianshuihe Fault and Miocene kinematics of SE Tibet, *Earth Planet. Sci. Lett.*, *465*, 1-15.

Zhuang, G., Y. Najman, S. Guillot, M. Roddaz, P.-O. Antoine, G. Métais, A. Carter, L. Marivaux, and S. H. Solangi (2015), Constraints on the collision and the pre-collision tectonic configuration between India and Asia from detrital geochronology, thermochronology, and geochemistry studies in the lower Indus basin, Pakistan, *Earth Planet. Sci. Lett.*, *432*, 363-373.

Zuza, A. V., and A. Yin (2016), Continental deformation accommodated by non-rigid passive bookshelf faulting: An example from the Cenozoic tectonic development of northern Tibet, Tectonophysics, 677-678(Supplement C), 227-240.

Table 1. Summary of sample details and AFT and AHe ages. For further information, see supporting information Tables S1-S5.

Borehole or outcrop	Sample number	Depth (m)	Formation/ Lithology	AFT age ± 1σ (Ma)	Non-projected AFT length ± se (μm)	AHe age (Ma) ‡
MB-profile						
Outcrop	OMB11	436*	K1 Sandstone	72.0±3.3	13.01±0.16	51.5, 31.0, 52.5, 30.6, 31.9, 33.2
	OMB12	181*	J2 Sandstone	70.8±3.0	12.99±0.17	32.9, 32.2, 22.9, 22.2, 38.0, 41.3, 32.0, 34.5, 24.1
Maoba-1 Borehole	MB1-4	-20	J2 Sandstone	61.3±3.4	12.47±0.16	27.2, 23.7, 29.3, 20.2
	MB1-1	-1518	J2 Sandstone	30.8±3.5	N.D.	16.7, 16.6, 16.9
	MB1-2	-1694	J1 Sandstone	31.2±3.0	N.D.	N.D.
	MB1-5	-2522	T3 Sandstone	23.0±2.3	N.D.	7.9
Maoba-3 Borehole	MB3-1-1	-2135	T3 Sandstone	N.D.§	N.D.	10.8, 11.8, 10.5
PG-profile						
Outcrop	OPG11	770*	J2 Sandstone	143.3±9.8	12.29±0.16	86.6, 67.3, 74.9, 85.3, 52.2, 76.8, 96.9, 33.4
	OPG15	64*	J2 Sandstone	71.5±3.9	13.16 ±0.10	51.0, 26.4, 38.4, 48.4
Puguang-2 Borehole	PG2-5	-370	J2 Sandstone	70.2±5.1	12.10±0.18	31.0, 58.6, 49.6, 49.3, 46.4, 31.1
	PG2-6	-1590	J2 Sandstone	42.4±3.2	12.00±0.16	16.2, 11.6, 16.8, 18.5
	PG2-2	-3026	T3 Sandstone	18.4±2.3	N.D.	N.D.
	PG2-3 /PG2-3-1	-3247	T3 Sandstone	11.4±1.5	11.27±0.38	1.1, 0.5
	PG2-4	-3416	T3 Sandstone	8.5±1.1	10.07±0.38	N.D.
Puguang-5 Borehole	PG5yx	-794	J2 Sandstone	N.D.§	N.D.	40.5, 25.5
	PG5-1-2	-2558	T3 Sandstone	N.D.§	N.D.	4.3, 2.8
	PG5-2-1	-3403	T3 Sandstone	N.D.§	N.D.	0.8, 1.4, 0.9

* Depths of outcrop samples are calculated by comparison to the surface elevations at the borehole sites.
‡ A list of AHe single grain ages.
se = standard error.
N.D. = not determined.

Figures and captions:

Figure 1. (a) Relief map of the Tibetan Plateau and adjacent areas. White arrows indicate present day motion of India, central Tibetan Plateau and Sichuan Basin relative to Siberia [*Zhang et al*., 2004]. Late Cretaceous – Cenozoic transtenional and extensional basins are marked as yellow polygons. Abbreviations: CB = Chengxian Basin; HB = Hanzhong Basin; JB = Jianghan Basin; NB = Nanyang Basin; SB = Sichuan Basin WB = Weihe Basin. The black rectangle marks the extent of panel (b). (b) Generalized geology map of the Sichuan Basin, after *SBGMR* [1991]. Structures shown are of Mesozoic- Cenozoic age. Note NE-striking folds in the eastern part of the basin. Also plotted are the available AFT and AHe thermochronological ages compiled by *Yang et al*. [2017]. (c) 3D view showing coincidence between fold belts in Mesozoic strata and topography (SRTM, http://srtm.csi.cgiar.org/) in eastern Sichuan Basin. See Fig. 1b for location.

Figure 2. Detailed surface geological map of the study area, showing dip measurements, location of boreholes and surface samples studied. The black line marks the seismic profiles presented in Fig. 3. The dashed line marks the surface projection of the blind fault shown by both surface geological mapping and seismic survey. Elevation contour is computed using a 200-m-interval.

Figure 3. (a) Seismic profile and topographic swath across the Doneyuezhai-Puguang

fault (for location see Fig. 2). The seismic profile shows two detachments involving Paleozoic – mid-Triassic and upper Triassic – lower Cretaceous strata, respectively, modified after *Tang et al*. [2008] and SINOPEC (China Petrochemical Corporation) in well completion reports for these boreholes. Faults associated with the lower and upper detachment are marked in red and yellow, respectively. Structures related to the lower detachment are cut by the upper one, which shortened post mid-Triassic strata. Locations of the four boreholes (MB-1, -3 and PG-2, -5) studied (vertical black lines) and sample locations (red and blue symbols) are marked on the profiles. For boreholes marked in brackets, their locations are projected approximations. Note that the grey areas above the seismically well-resolved strata are shallow 'noisy' intervals where no meaningful seismic data are available. Note this panel is vertically exaggerated by ~2.5 times. (b) Lateral comparison of sample (both borehole and outcrop) depths and borehole stratigraphy, showing 0.8-1.3-km-vertical offset of stratigraphic formations between the boreholes on different sides of the shortening structure (the Dongyuezhai-Puguang fault, Fig. 2). Borehole stratigraphy is based on SINOPEC (China Petrochemical Corporation) well completion reports.

Figure 4. Plots of AFT age (a) and non-projected mean track lengths (b) and AHe age (c) down borehole. Errors shown are ± 1σ. In panel (c), the red and blue envelopes, include ~90% of the AHe data, illustrating the different age-depth relationships between the MB- and PG-profiles.

Figure 5. Thermal modeling results and comparison between AFT and AHe observations and model predictions for the MB-profile (a-1 and a2) and PG-profile (b-1 and b-2). In panels a-1 and b-1, the thermal history of the uppermost sample is plotted in blue, the lowermost sample in red, and intermediate samples in grey. For the uppermost thermal history, thin blue lines depict 95% credible intervals, reflecting the uncertainty in the inferred thermal history alone. For the lowermost thermal history, thin red lines show the 95% credible intervals, reflecting combined uncertainties in the inferred thermal history and offset parameters (see Supporting Information for details). Black boxes and thick lines mark geological constraints used in the modeling. In panels a-2 and b-2, comparisons between observed and modeled AFT ages, projected mean track lengths and corrected AHe ages are plotted. Histogram plots in the upper and lower parts show the comparison between observed (O) and predicted (P) length distributions and mean lengths. In these plots, the red curves denote the predicted distribution, with the 95% credible intervals marked in green. Thermal history modeling for combined data from the MB-profile indicates a distinct cooling episode between ~35-28 Ma (marked by gray shading), followed by a phase of thermal quiescence, while the PG-profile displays a persistent linear cooling history.

Figure 6. Deformation sequence in the eastern Tibetan Plateau and the Sichuan Basin. In late Eocene time, the eastern Sichuan Basin was shortened together with the eastern

Tibetan Plateau. In late Miocene time, deformation retreated westwards to the Longmen Shan and Xianshuihe faults, and other areas further west. Shaded area marks the Mesozoic foreland Sichuan Basin, underlain by a relatively strong lithosphere compared to the eastern Tibetan Plateau to the west and the Yangtze block to the east. The thick black line marks the location of the profile shown in Fig. 7.

Figure 7. Structural interpretation for the late Eocene – Oligocene (a) and late Miocene (b) phases of deformation. (a) Late Eocene – Oligocene eastward extrusion of the eastern Tibetan Plateau is accommodated by crustal shortening structures extending from the Longmen Shan to the eastern Sichuan Basin, where reverse faults are east-verging (upper) or the west-verging (lower), as marked by red dashed rectangles. (b) Late Miocene time witnessed a retreat of deformation towards the plateau interior, which might be a response to either out-of-sequence deformation, facilitated by enhanced late Miocene erosion in the plateau margin (upper), or lower crustal channel flow, as proposed by previous studies (lower). The thick horizontal black line marks the region of enhanced late Miocene erosion [*Godard et al.*, 2009; *Wang et al.*, 2012a; *Tian et al.*, 2013; *Tian et al.*, 2015].

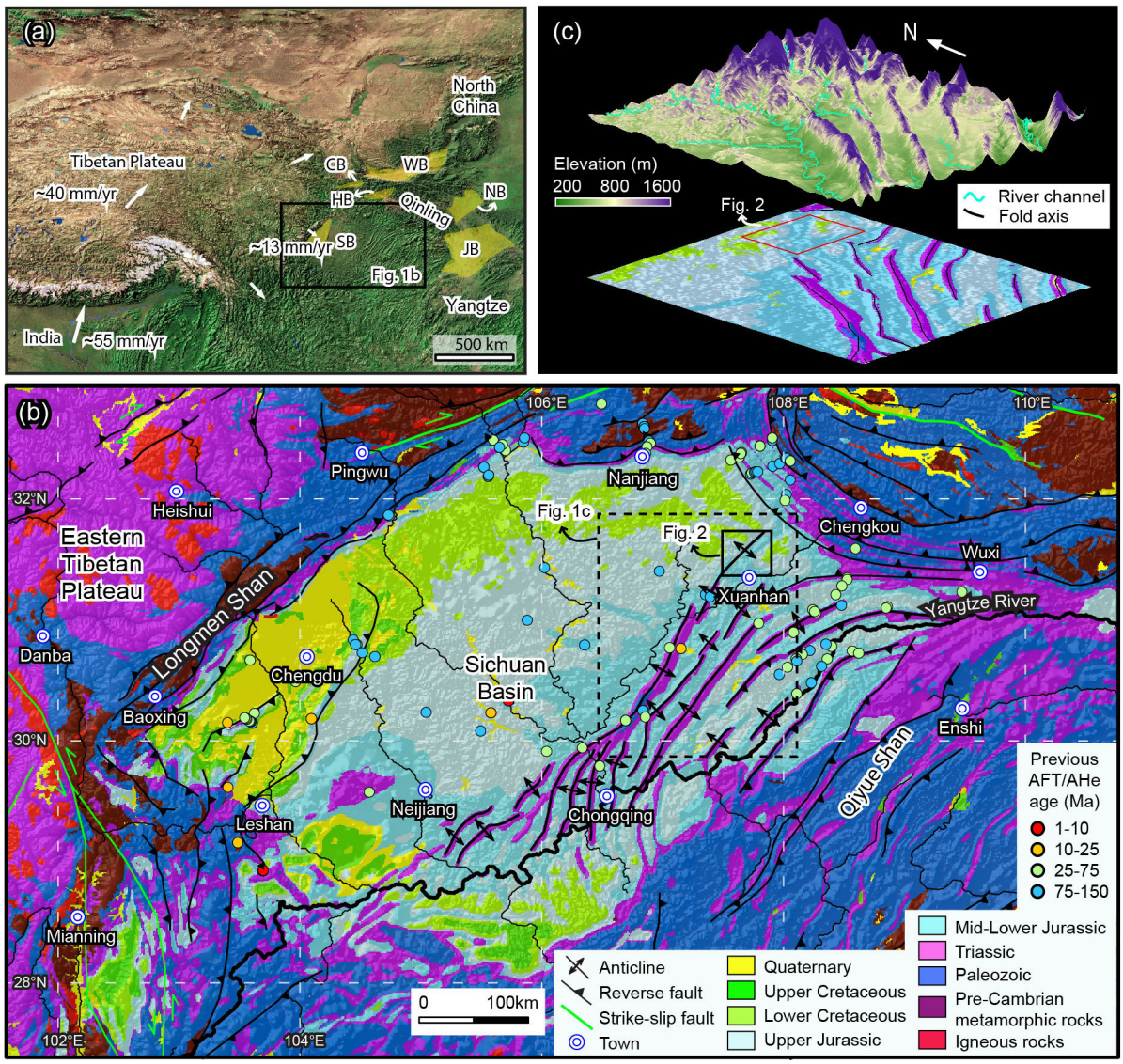

2017JB015049-f01-z-.jpg

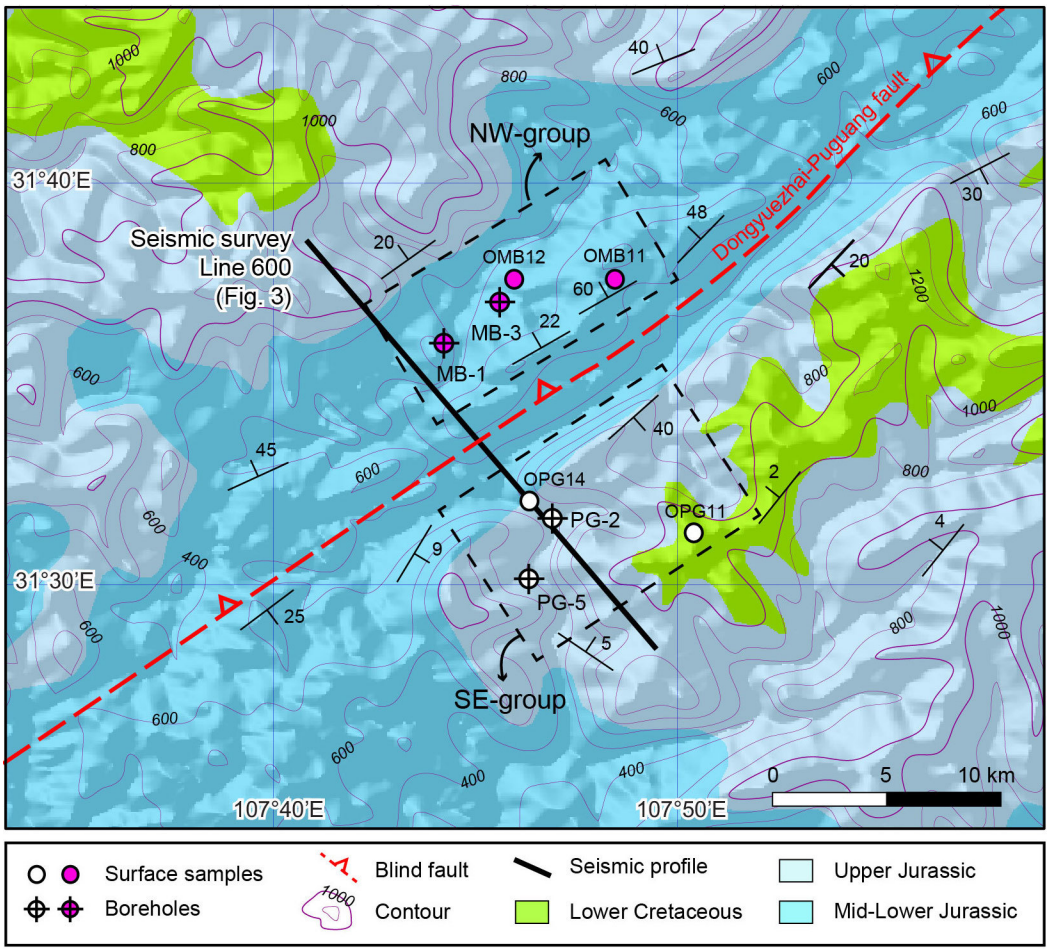

2017JB015049-f02-z-.jpg

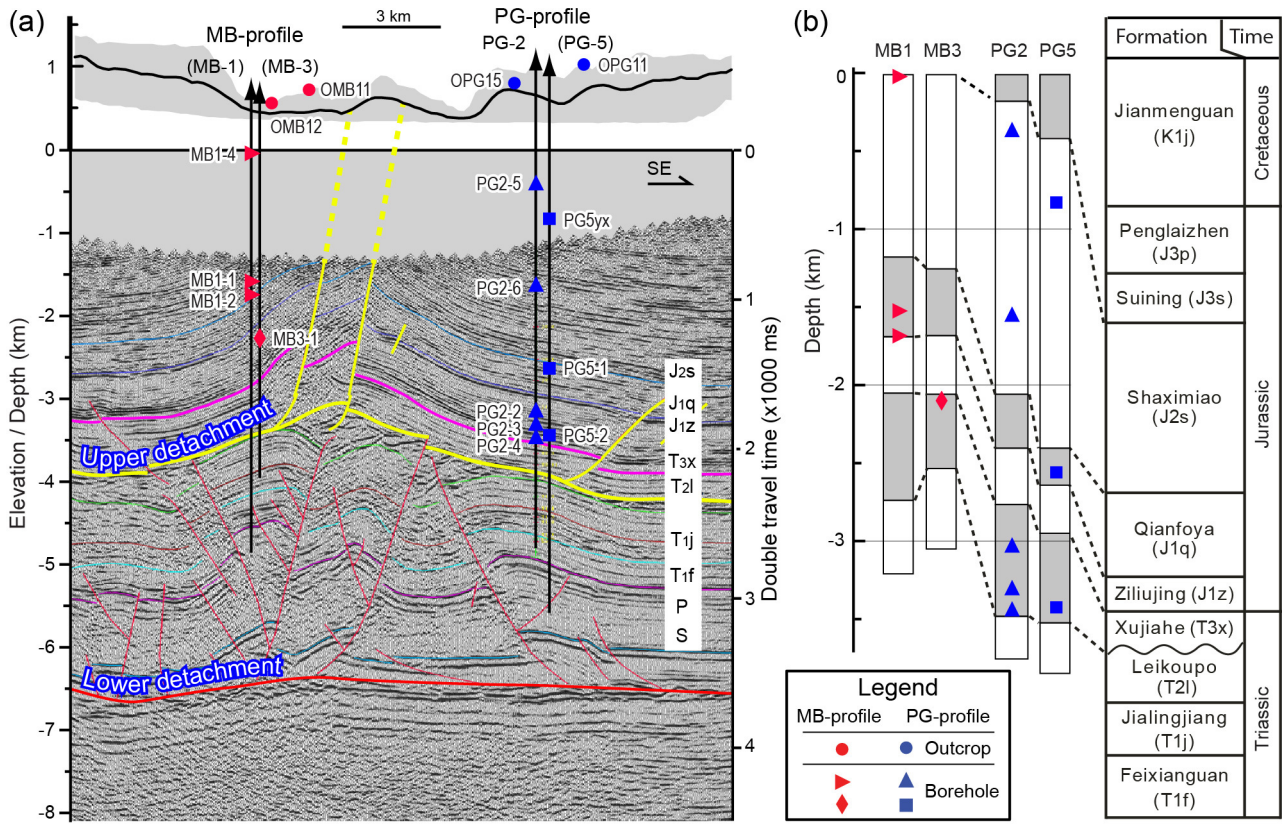

2017JB015049-f03-z-.jpg

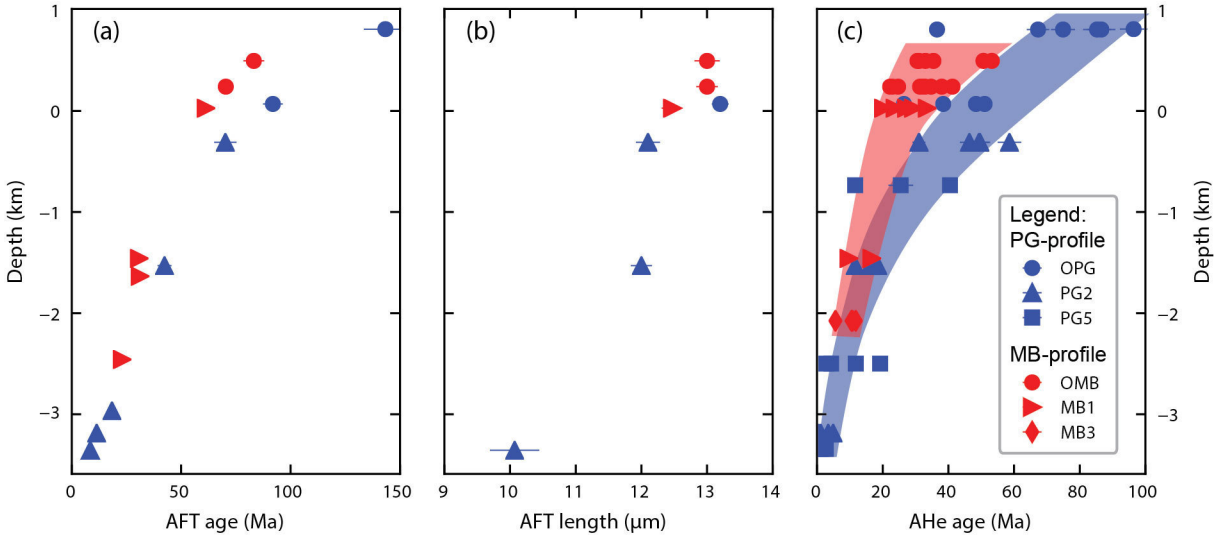

2017JB015049-f04-z-.jpg

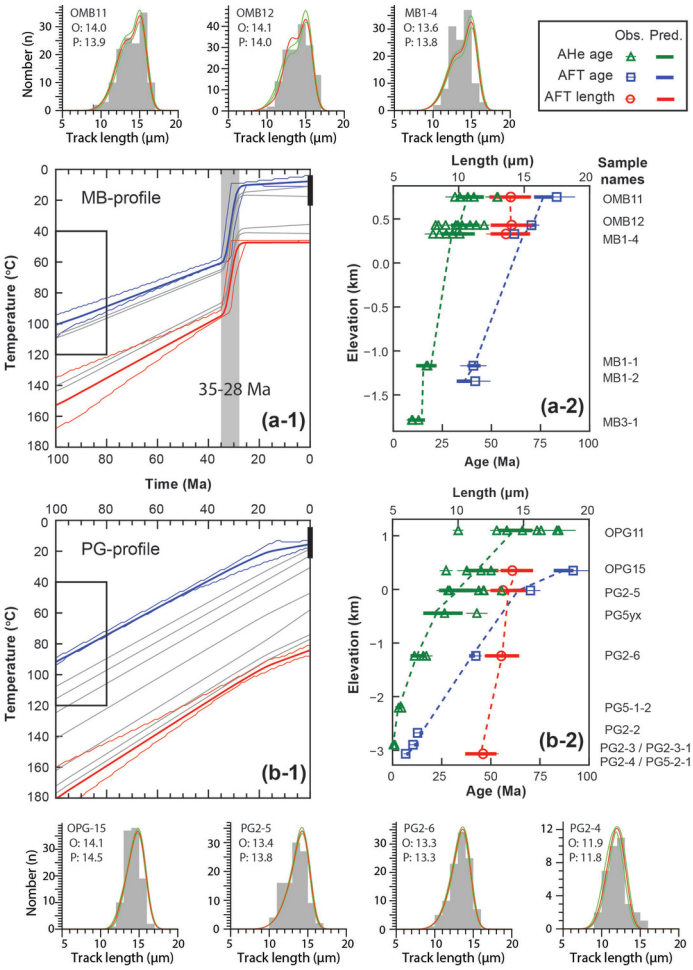

2017JB015049-f05-z-.jpg

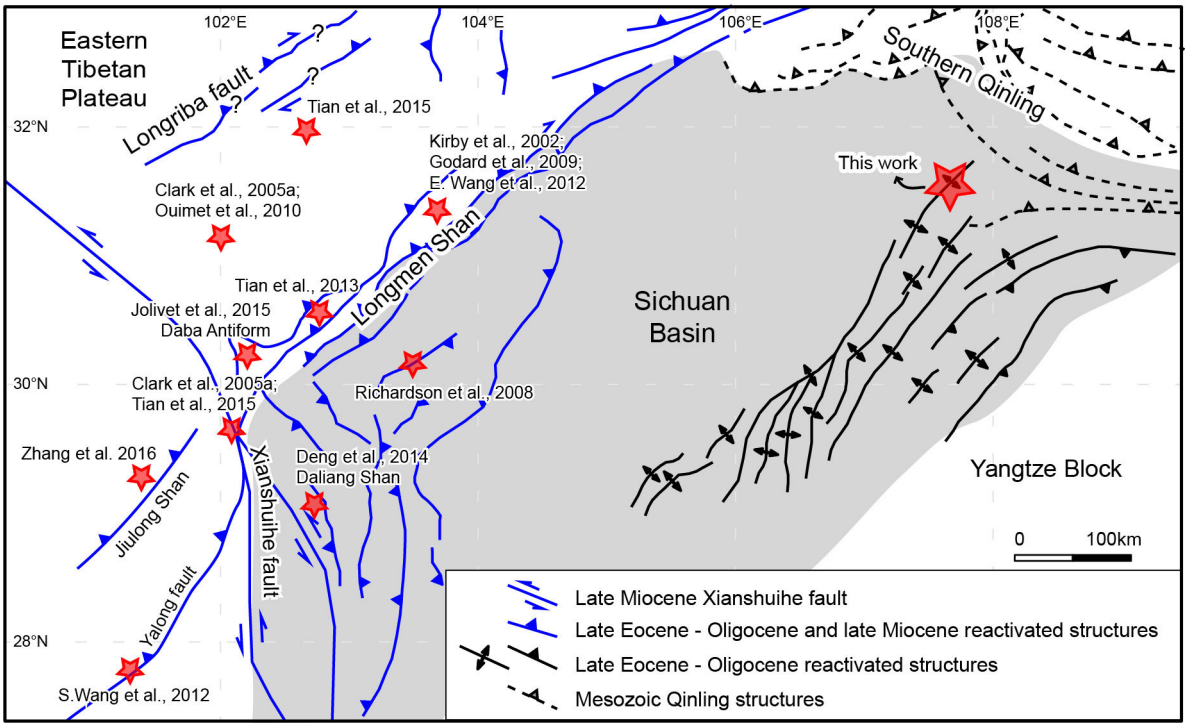

2017JB015049-f06-z-.jpg

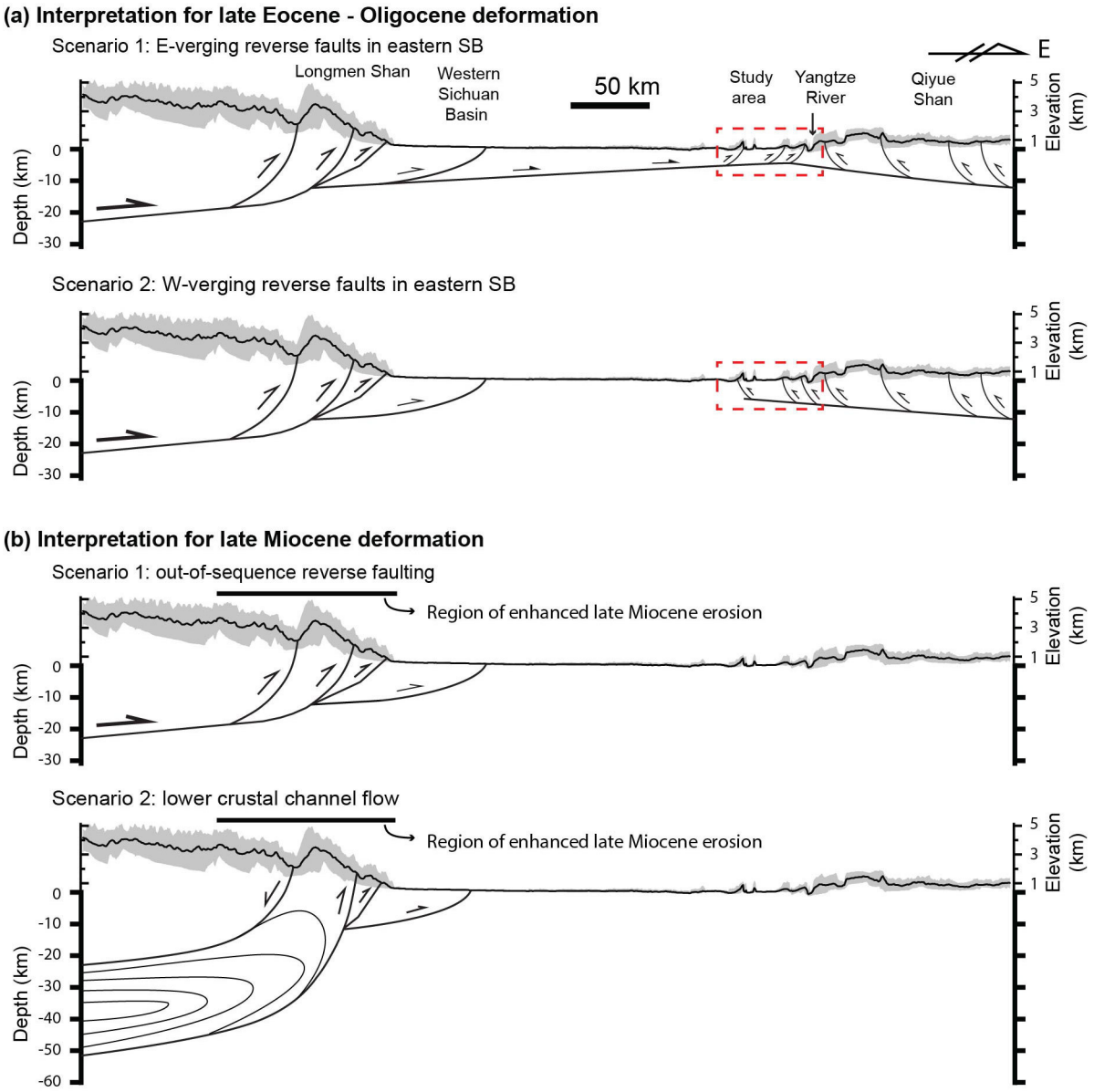

2017JB015049-f07-z-.jpg